

PHYSICS MODEL OF AN ALLISON PHASE-SPACE SCANNER, WITH APPLICATION TO THE FRIB FRONT END*

Chun Yan Jonathan Wong[†], National Superconducting Cyclotron Laboratory, East Lansing, USA
 Scott Cogan, Yue Hao, Steven Lidia, Steven M. Lund, Tomofumi Maruta[‡], Diego Omitto,
 Peter Ostroumov, Eduard Pozdeyev, Haitao Ren, Rebecca Shane, Takashi Yoshimoto, Qiang Zhao
 Facility for Rare Isotope Beams, East Lansing, USA

Abstract

We study Allison-type phase-space scanners by extending analytic models to include two important geometric features that are conventionally omitted, namely asymmetric slit-plate to dipole-plate gaps at the two ends and finite slit-plate thickness. Their effects can be significant for high-resolution Allison scanners and lead to two corrections in the measurement data relative to more idealized descriptions: 1) a change in the voltage-to-angle conversion relation, and 2) a data point weight compensation factor. These findings are corroborated by numerically integrated single-particle trajectories in a realistic 2D field map of the device. The improved model was applied to the Allison scanner used to measure a 12 keV/u heavy-ion beam in the front-end of the Facility for Rare Isotope Beams (FRIB) at Michigan State University. Preliminary measurements show that the improved model results in significant ($\geq 10\%$) modifications to beam moments, thus rendering the corrections important for accurate phase-space characterizations.

INTRODUCTION

Allison scanners [1] are widely used to efficiently measure slit-transmitted phase-space projections of low-energy beams. An Allison scanner (see Fig. 1) consists of an entrance slit-plate (slit width s), an aligned exit slit-plate (slit width s) with an integrated Faraday cup, and a bipolar-biased electric dipole (voltage V_0) placed between the two slits. The scanner is translated mechanically (typically in steps) to change the slit position, and the dipole voltage V_0 is varied to select transmittable angles by varying the bending strength. For a particular coordinate and dipole voltage, the scanner samples a point in the beam phase-space. The density of the point is taken to be proportional to the current collected at the Faraday cup.

Idealized analytic formulas relating Allison scanner geometry and voltages to phase-space measures were derived in Refs. [1,2]. These idealized results assume thin slit-plates, an ideal (no-fringe) dipole field, and a symmetric geometry. This paper extends idealized model results by considering two additional geometric features that can lead to significant corrections: 1) asymmetric slit-plate to dipole-plate gaps at the two ends, and 2) finite slit-plate thickness.

Asymmetry commonly arises, probably unintentionally, in Allison scanners because relief cuts on thick entrance- and exit-plates have been made in the same direction [3,4]. This asymmetry is also present in the FRIB Allison scanner where relief cuts on both plates face the incoming beam as shown in Fig. 1. Due to this issue, the effective slit-plate to dipole-plate gap on the exit end is more than double that on the entrance end. We find such asymmetries significantly impact angle selection calibration with V_0 .

Slit-plate thickness can be neglected when it is much smaller than the slit width. This idealization can break down as Allison scanners decrease slit widths to improve resolution. Recent examples include slit widths of $s \leq 100 \mu\text{m}$ planned at GSI FAIR [5] and $s = 38 \mu\text{m}$ implemented at TRIUMF [6]. Fig. 1 details the slit plate presently employed in the FRIB scanner where $s = 60 \mu\text{m}$ and the effective (not including irrelevant thickness spanning the 30° relief cut) plate-thickness is $254 \mu\text{m}$. This approximately 4 : 1 aspect ratio is effectively a small channel, which can scrape particles that would have passed through a slit-plate with no thickness.

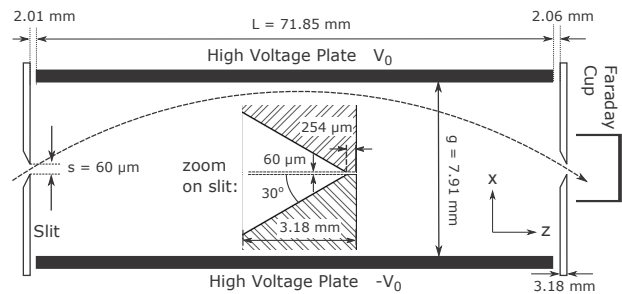


Figure 1: FRIB Allison scanner geometry.

ANALYTIC MODEL

Four geometric models of an Allison scanner are presented in Fig. 2. The models cover combinations of symmetric/asymmetric end-plate to slit-plate gaps with thin/thick slit-plates to study effects of asymmetry and slit-plate thickness. As illustrated in the Fig. 2, a range of angles can be transmitted at each voltage setting due to the finite slit width. We define:

x'_{ref} : the angle at which a particle enters and exits the chamber at the same x -position,

$x'_{\text{max/min}}$: maximum/minimum transmittable angle,

$\Delta x' = x'_{\text{max}} - x'_{\text{min}}$: angular resolution,

* Work supported by the U.S. DOE Office of Science under Cooperative Agreement DE-SC0000661 and the NSF under Grant No. PHY-1102511.

[†] wong@nsl.msu.edu

[‡] On leave from KEK/J-PARC

where $x' \equiv dx/dz$ and $x = 0$ corresponds to the device center-line. Note that the points at which extreme trajectories touch the slits are shifted when the slits have finite thickness.

Particle transmission efficiency can be understood as follows. For any $x' \in [x'_{\min}, x'_{\max}]$, one can find a trajectory with initial angle x' that allows the particle to pass through both slits. Imagine shifting that trajectory along the x -axis, which is equivalent to changing the initial x -position. Among all shifted particles that enter the entrance slit with angle x' , some are transmitted while others are scraped. This gives rise to a transmitted fraction (T) that depends on the initial angle value of x' which sets the shape of the trajectory. Assuming a uniform distribution of particle x -coordinates across the slit, we define $p(x') = (\text{no. transmitted})/(\text{no. entering})$, where $p(x'_{\text{ref}})$ is closest to unity and $p(x'_{\max}) = p(x'_{\min}) = 0$. Assuming uniform distribution in x' for $x' \in [x'_{\min}, x'_{\max}]$, $T(x'_{\text{ref}}) = \int_{x'_{\min}}^{x'_{\max}} p(x') dx' / \int_{x'_{\min}}^{x'_{\max}} dx'$ is the overall fraction of particles within the angular range that is transmitted.

We analytically calculate particle trajectories in the models by treating the biased plates as perfect hard-edge dipoles that extend over the axial length of the plates. Angular ranges $x'_{\max, \min}$ are determined by solving for the limiting particles that touch the entrance and exit slits at the coordinates illustrated in Fig. 2. Results are summarized in Table 1. \mathcal{E} denotes the particle kinetic energy.

NUMERICAL MODEL

A Python code is employed to numerically integrate particle equations of motion in a realistic 2D field map of the device geometry that is generated from the electrostatic field code POISSON [7]. E_x and E_z electric field data is exported from POISSON onto a high-resolution $x-z$ mesh with $dx = dz = 0.2$ mm, and imported into the Python code. Fields at the particle position are calculated using linear area interpolation from the gridded field data [8]. Image charges, beam space charge, and scattering effects are neglected. Non-relativistic equations of motion are exactly transformed from time t to axial coordinate z obtaining:

$$\frac{d}{dz} \begin{bmatrix} x \\ t \\ x' \\ t' \end{bmatrix} = \begin{bmatrix} x' \\ t' \\ \left(\frac{qE_x}{m} - \frac{qE_z}{m} x' \right) t'^2 \\ -\frac{qE_z}{m} t'^3 \end{bmatrix}$$

The state vector describing the particle trajectory is advanced using the ode package within Scientific Python (SciPy) [9] for specified initial particle coordinate x , angle x' , and dipole voltage V_0 (field data scaled). The code takes into account scraping on all boundaries. To solve for $x'_{\max, \min}$, we note that the corresponding trajectory must touch the slits at two points (see Fig. 2). We employ a numerical root-finding procedure to solve for the initial x' that connects the upstream point to the downstream point. x'_{ref} is solved analogously with the condition $x = 0$ at both ends.

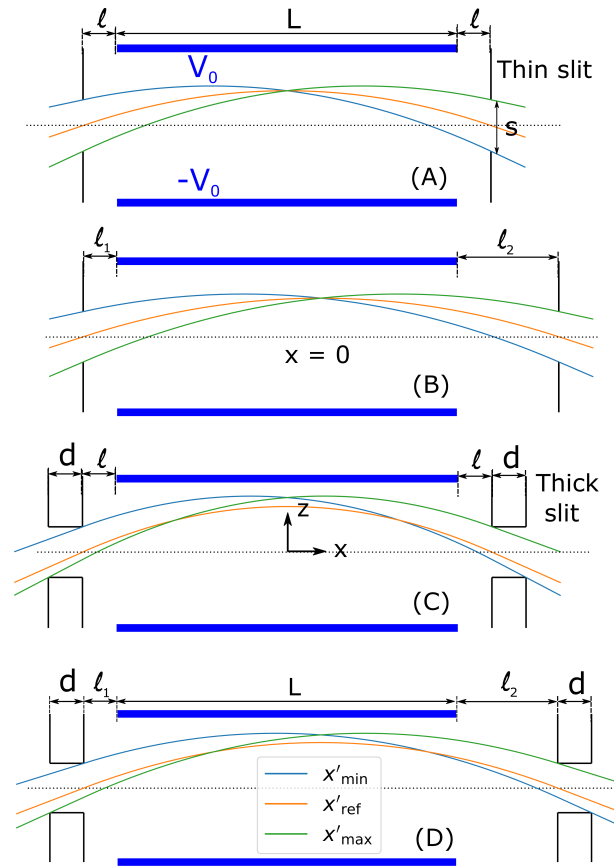


Figure 2: Four geometric models. Model A: zero end distances, thin plate; Model B: non-zero end distances, thin plate; Model C: zero end distances, thick plate; Model D: non-zero end distances, thick plate.

DATA ANALYSIS: TWO CORRECTIONS

The results from analytic and simulation studies reveal two significant corrections on measurement data from Allison scanners relative to ideal symmetric, thin-plate results [1,2]. The ideal results are summarized in column A of Table 1. Note that the ideal results allow symmetric slit-plate to dipole-plate gaps upstream and downstream. One correction alters the dipole voltage (V_0) to selected angle (x'_{ref}) relation of the device due to asymmetric gaps. The other correction characterizes how finite slit-plate thickness alters the transmitted current as a function of x'_{ref} . We illustrate these effects for the FRIB Allison scanner geometry shown in Fig. 1 for an Ar^{9+} ion with kinetic energy $\mathcal{E} = 12$ keV/u.

Voltage-to-Angle Relation

As shown in Table 1, when end distances are asymmetric, the reference angle x'_{ref} has an additional factor $(L+2l_2)/(L+l_1+l_2)$ relative to the ideal model results (column A) which deviates from unity. For the FRIB Allison scanner, $l_1 = 2.01$ mm and $l_2 = (2.06 + 3.18 - 0.254)$ mm = 4.99 mm. So the relief cuts generate significant effective asymmetry. In Fig. 3, x'_{ref} versus V_0 is plotted for numerical (realistic), ideal analytic (Table 1, column A), and improved analytic (Table 1,

Table 1: Analytic Results Corresponding to the Geometric Models in Fig. 2

Model	A	B	C	D
End-gap distances Plate	Symmetric Thin	Asymmetric Thin	Symmetric Thick	Asymmetric Thick
x'_{ref}	$\frac{1}{2} \frac{qV_0 L}{g\mathcal{E}}$	$\frac{1}{2} \frac{qV_0 L}{g\mathcal{E}} \left(\frac{L+2l_2}{L+l_1+l_2} \right)$	$\frac{1}{2} \frac{qV_0 L}{g\mathcal{E}}$	$\frac{1}{2} \frac{qV_0 L}{g\mathcal{E}} \left(\frac{L+2l_2}{L+l_1+l_2} \right)$
$x'_{\text{max}} - x'_{\text{ref}}$	$\frac{s}{L+2l}$	$\frac{s}{L+l_1+l_2}$	$\frac{s-x'_{\text{ref}}d}{L+2l+d}$	$\frac{s-x'_{\text{ref}}d}{L+l_1+l_2+d}$
$x'_{\text{ref}} - x'_{\text{min}}$	$\frac{s}{L+2l}$	$\frac{s}{L+l_1+l_2}$	$\frac{s-x'_{\text{ref}}d}{L+2l+d}$	$\frac{1}{L+l_1+l_2+d} \left(s - \frac{L+2l_1}{L+2l_2} x'_{\text{ref}}d \right)$
$\Delta x'$	$\frac{2s}{L+2l}$	$\frac{2s}{L+l_1+l_2}$	$\frac{2s}{L+2l+d} \left(1 - \frac{x'_{\text{ref}}d}{s} \right)$	$\frac{2s}{L+l_1+l_2+d} \left(1 - \frac{L+l_1+l_2}{L+2l_2} \frac{x'_{\text{ref}}d}{s} \right)$
$p(x')$ for $x' \geq x'_{\text{ref}}$		$\frac{x' - x'_{\text{ref}}}{x'_{\text{max}} - x'_{\text{ref}}}$		$\frac{x' - x'_{\text{ref}}}{x'_{\text{max}} - x'_{\text{ref}}} \left(1 - \frac{x'_{\text{ref}}d}{s} \right)$
$p(x')$ for $x' < x'_{\text{ref}}$		$\frac{x'_{\text{ref}} - x'}{x'_{\text{ref}} - x'_{\text{min}}}$		$\frac{x'_{\text{ref}} - x'}{x'_{\text{ref}} - x'_{\text{min}}} \left(1 - \frac{x'_{\text{ref}}d}{s} \right)$
$T(x'_{\text{ref}})$	$\frac{1}{2}$	$\frac{1}{2}$	$\frac{1}{2} \left(1 - \frac{x'_{\text{ref}}d}{s} \right)$	$\frac{1}{2} \left(1 - \frac{x'_{\text{ref}}d}{s} \right)$

column B or D) models. The improved and numerical model results are almost identical, giving slopes of 88.5 mrad/kV and 88.4 mrad/kV, respectively. The minimal difference suggests that fringe field effects of the dipole electric fields near the slits have little impact on the transmitted particle trajectories. The ideal expression commonly used shows a 4% deviation relative to numerical model results with a slope of 85.3 mrad/kV, thereby showing significant impact of the effective asymmetry.

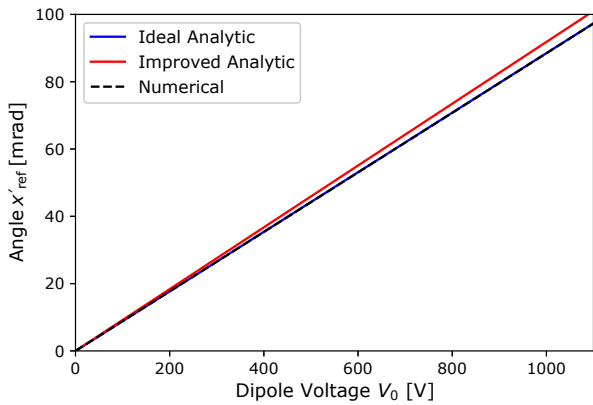


Figure 3: Voltage-to-angle relation for the selected beam.

Voltage-Dependent Weight Compensation

As evident from results in Table 1, for thick slit-plates, the angular resolution $\Delta x'$ and transmission ratio T both decrease linearly as a function of x'_{ref} . This has important implications.

Phase-space scans are typically performed by measuring the current at regular discrete steps in slit position (x -origin shift) and voltage (V_0). The data is represented by a grid in phase-space where each grid is a rectangle of size (position step) \times (voltage step). In general, grid dimensions

will not coincide with the spatial and angular acceptance of the device. Assuming a uniform distribution of particles within each grid, to calculate the actual beam current that falls within each phase-space grid, the current of data points should be multiplied by:

$$\frac{\text{Angular step}}{T \times \Delta x'} \times \frac{\text{Spatial step}}{\text{slit size}}.$$

Note that the multiplication of T and $\Delta x'$ renders the correction factor *quadratic* in $x'_{\text{ref}}d/s$. When the plate-thickness to slit-width ratio d/s is small, this factor is small, and all data points are scaled almost uniformly as in the case of the ideal analysis. However, when slit-widths are small, $x'_{\text{ref}}d/s$ is large, causing sampled data points to be rescaled differently depending on the angle (x_{ref}) of the data point. In Fig. 4, the angular resolution $\Delta x'$, transmission factor T , and the angular correction factor $\propto 1/(T\Delta x')$ are plotted as a function of dipole voltage V_0 for the FRIB Allsion scanner. Curves for numerical (accurate), ideal analytic (Table 1, Column A), and improved (Table 1, Column D) analytic model results are shown. The correction introduced by the effect of finite slit-plate thickness can be substantial. For example, in the FRIB device, when $x'_{\text{ref}} = 70$ mrad,

$$\left(1 - \frac{L+l_1+l_2}{L+2l_2} \frac{x'_{\text{ref}}d}{s} \right) \left(1 - \frac{x'_{\text{ref}}d}{s} \right) \approx 0.5.$$

Therefore, if we apply the ideal model where all data points have equal weights, 0-mrad data points would wrongly weigh twice as much as ± 70 -mrad data points. Failure to rectify the weights would distort the measurement with increasing amplitude as characteristic beam angles increase.

FRIB APPLICATION

The front-end of the Facility for Rare Isotope Beams (FRIB) [10] commenced early commissioning activities in

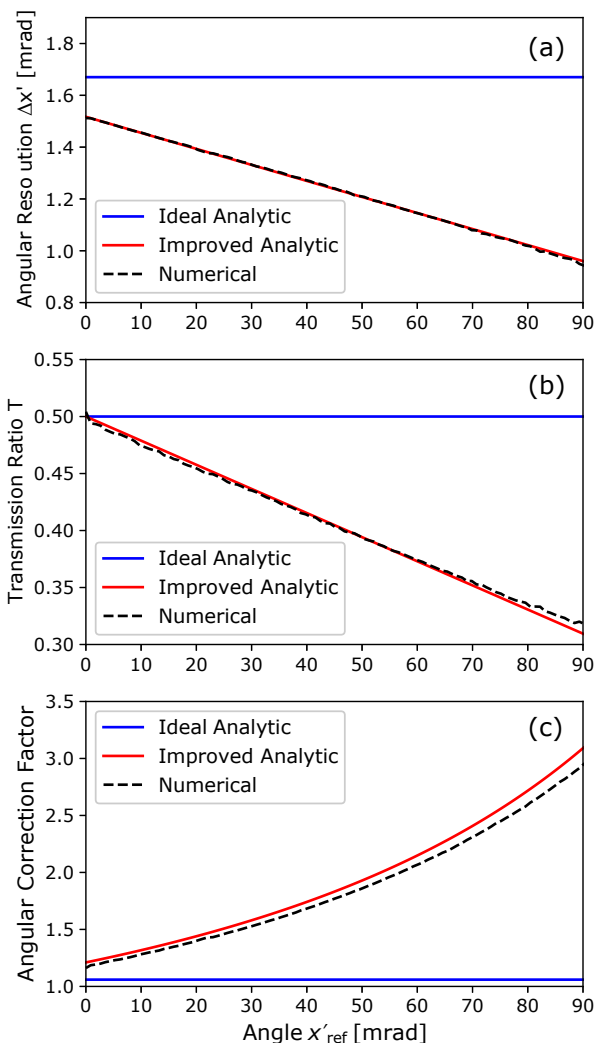


Figure 4: Plots of a) angular resolution $\Delta x'$, b) transmission ratio T , and c) angular correction factor as a function of x'_{ref} .

June 2017. Here we apply analytic model (Table 1, Column D) results to analyze changes in measurements of beam phase-space properties for a y -plane Allison scanner after species separation. Preliminary measurements for a Ar^{9+} ion beam with $20\ \mu\text{A}$ (Faraday cup measure) are used to illustrate corrections. The ions are produced in an ECR source [11] with a 15 kV extraction voltage. The beam then traverses a short section with solenoid focusing and an electrostatic gap biased to accelerate the target ion species to 12 keV/u. Species are separated in a 90° magnetic dipole, downstream of which is an electrostatic quadrupole triplet before measurement by the Allison scanner. A y - y' phase-space projection (with corrections) is shown in Fig. 5. The scan is performed with spatial steps of $\Delta y = 1\ \text{mm}$ and voltage steps of $\Delta V_0 = 20\ \text{V}$. We average data in a region with no beam to establish the background noise level, which is then subtracted from data points of interest. Corresponding first- and second-order beam moments including the normalized rms emittance are listed in Table 2. Moments

Table 2: Measured FRIB Beam Moments Corresponding to Fig. 5, Calculated with and without Corrections. ($\dots\%$) indicate percent deviations of corrected relative to uncorrected results.

Correction	None	x'_{ref}	$x'_{\text{ref}} + \text{Weight}$
$\langle y \rangle$ [mm]	-14.7	-14.7	-14.6 (0.4%)
$\langle y' \rangle$ [mrad]	6.95	7.21	7.55 (8.6%)
$\langle y^2 \rangle$ [mm^2]	6.49	6.49	6.97 (7.4%)
$\langle yy' \rangle$ [mm-mrad]	20.2	21.0	22.9 (13.4%)
$\langle y'^2 \rangle$ [mrad^2]	90.3	97.3	105.1 (16.4%)
$\varepsilon_{n\text{-rms}}$ [mm-mrad]	0.0675	0.0700	0.0729 (8.1%)

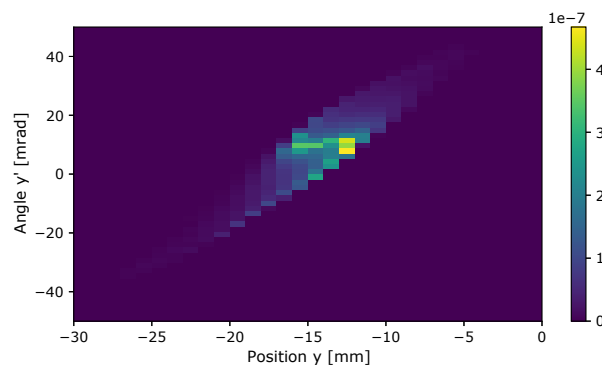


Figure 5: Measured FRIB y - y' phase-space projection (range truncated to better illustrate).

are computed both with (Table 1, Column D) and without (ideal model; Table 1, Column A) corrections to illustrate the deviation. The large centroid offset appears to be related to scanner reference coordinate offset (under investigation). All second-order moments have centroids subtracted, i.e., $\langle y^2 \rangle = \langle (y - \langle y \rangle)^2 \rangle$. We observe a $\geq 10\%$ difference in beam moments, thus confirming the importance of corrections for accurate measurements.

Lastly, we note that although the analysis was made for an Ar^{9+} ion, all results hold identically for other ions with 12 keV/u energy if the dipole voltage V_0 is rescaled by the dimensionless charge-to-mass ratio (A/Q) to keep the acceleration constant:

$$V_0 \rightarrow V_0 \frac{9}{39.95} \left(\frac{A}{Q} \right).$$

CONCLUSION

We identified two important effects for high-resolution Allison scanners that arise from geometric features. Asymmetric dipole-plate to slit-plate gaps at the two ends alter the voltage-to-angle relation for the selected beam, whereas slit-plate thickness \geq slit width requires a data point weight correction that is quadratic in voltage. These effects can significantly change results of phase-space measurements relative to idealized analysis commonly employed. We modeled these effects with analytic formulas that have been verified by

a more exact numerical model. Applying derived correction factors to preliminary Allison scanner measurement data in FRIB led to significant ($\geq 10\%$) changes in beam moments. Since the effects grow with particle angle, corrections can be larger or smaller depending on the effective angular extents of the distribution measured.

REFERENCES

- [1] P. W. Allison, J. D. Sherman, and D. B. Holtkamp, "An Emittance Scanner for Intense Low-Energy Ion Beams", *IEEE Transactions on Nuclear Science*, vol. 30, no. 4, pp. 2204-2206, 1983
- [2] M.P. Stockli, R.F. Welton, R. Keller, and M. Leitner, "Emittance studies with an Allison scanner", *Rev. Sci. Instrum.*, 77(3), p.03B706, 2006
- [3] M.P. Stockli *et al.*, "Low-energy emittance studies with the new SNS Allison emittance scanner", in *Proc. 23rd Particle Accelerator Conf. (PAC'09)*, Vancouver, Canada, May 2009.
- [4] R. D'Arcy, M. Alvarez, J. Gaynier, L. Prost, V. Scarpine, and A. Shemyakin, "Characterisation of the PXIE Allison-Type Emittance Scanner", *Nucl. Instr. Meth. A*, vol. 815, pp. 7-17, 2014
- [5] C. Ullmann *et al.*, "Status and computer simulations for the front end of the proton injector for FAIR", in *Proc. IPAC'14*, Dresden, Germany (2014)
- [6] A. Laxdal *et al.*, "Allison Scanner Emittance Diagnostic Development at TRIUMF", in *Proc. LINAC2014*, paper THIOC02, Geneva, Switzerland (2014)
- [7] Poisson/Superfish web site, http://laacg.lanl.gov/laacg/services/download_sf.phtml
- [8] C. K. Birdsall and A. B. Langdon, *Plasma physics via computer simulations*, McGraw-Hill Book Company, New York (1985).
- [9] E. Jones *et al.*, "SciPy: Open source scientific tools for Python", <http://www.scipy.org/>.
- [10] J. Wei, "The FRIB Superconducting Linac - Status and Plans", in *Proc. LINAC2016*, paper M01A01, East Lansing, MI, USA, September 2016.
- [11] G. Machicoane, D. Cole, J. Ottarson, J. Stetson, and P. A. Zavadzky, "ARTEMIS-B: A room-temperature test electron cyclotron resonance ion source for the National Superconducting Cyclotron Laboratory at Michigan State University", *Rev. Sci. Instrum.* 77, 03A322 (2006)